

LETTER TO THE EDITOR

Mini-moons from horseshoes: A physical characterization of 2022 NX₁ with OSIRIS at the 10.4 m Gran Telescopio Canarias[★]

R. de la Fuente Marcos¹, J. de León^{2,3}, C. de la Fuente Marcos⁴, J. Licandro^{2,3}, M. Serra-Ricart^{2,3}, and A. Cabrera-Lavers^{5,2,3}

¹ AEGORA Research Group, Facultad de Ciencias Matemáticas, Universidad Complutense de Madrid, Ciudad Universitaria, E-28040 Madrid, Spain

² Instituto de Astrofísica de Canarias (IAC), C/ Vía Láctea s/n, E-38205 La Laguna, Tenerife, Spain

³ Departamento de Astrofísica, Universidad de La Laguna, E-38206 La Laguna, Tenerife, Spain

⁴ Universidad Complutense de Madrid, Ciudad Universitaria, E-28040 Madrid, Spain

⁵ GRANTECAN, Cuesta de San José s/n, E-38712 Breña Baja, La Palma, Spain

Received 21 November 2022 / Accepted 21 January 2023

ABSTRACT

Context. The near-Earth orbital space is shared by natural objects and space debris that can be temporarily captured in geocentric orbits. Short-term natural satellites are often called mini-moons. Reflectance spectroscopy can determine the true nature of transient satellites because the spectral signatures of spacecraft materials and near-Earth asteroids (NEAs) are different. The recently discovered object 2022 NX₁ follows an Earth-like orbit that turns it into a recurrent but ephemeral Earth companion. It has been suggested that 2022 NX₁ could have an artificial origin or be lunar ejecta.

Aims. Here, we use reflectance spectroscopy and *N*-body simulations to determine the nature and actual origin of 2022 NX₁.

Methods. We carried out an observational study of 2022 NX₁, using the OSIRIS camera spectrograph at the 10.4 m Gran Telescopio Canarias, to derive its spectral class. *N*-body simulations were also performed to investigate how it reached NEA space.

Results. The reflectance spectrum of 2022 NX₁ is neither compatible with an artificial origin nor lunar ejecta; it is also different from the V type of the only other mini-moon with available spectroscopy, 2020 CD₃. The visible spectrum of 2022 NX₁ is consistent with that of a K-type asteroid, although it could also be classified as an Xk type. Considering typical values of the similar albedo of both K-type and Xk-type asteroids and its absolute magnitude, 2022 NX₁ may have a size range of 5 to 15 m. We confirm that 2022 NX₁ inhabits the rim of Earth's co-orbital space, the 1:1 mean-motion resonance, and experiences recurrent co-orbital engagements of the horseshoe-type and mini-moon events.

Conclusions. The discovery of 2022 NX₁ confirms that mini-moons can be larger than a few meters and also that they belong to a heterogeneous population in terms of surface composition.

Key words. minor planets, asteroids: general – minor planets, asteroids: individual: 2022 NX₁ – techniques: spectroscopic – methods: numerical – celestial mechanics

1. Introduction

The Moon is Earth's only permanent natural satellite but over 22,000 artificial objects (active spacecraft and space debris) of all sizes also orbit our planet (McDowell 2020).¹ In addition, passing bodies may be captured in geocentric orbits if they move at very low relative velocity inside the Hill radius of Earth, 0.0098 AU; these include both small natural bodies (Granvik et al. 2012) and hardware originally inserted in cislunar or interplanetary space (Cano et al. 2019).² Natural temporarily captured orbiters of Earth or mini-moons appear to be rare, difficult to spot objects (Fedorets et al. 2020). Prior to 2022, only three small natural bodies had been identified crossing into the region

defined by negative geocentric energy. Most captured objects are eventually confirmed as returning space debris.

Reflectance spectroscopy can help to determine the true nature of transient satellites because the spectral signatures of spacecraft materials and rocky asteroids are different. This technique is routinely used to identify space debris unambiguously (see for example Jorgensen 2000; Jorgensen et al. 2004; Schildknecht 2007; Vananti et al. 2017; Cowardin et al. 2021).

Spectral observations led to confirm that J002E3, an object found orbiting Earth in 2002, was the upper S-IVB stage of Apollo 12 which launched on November 14, 1969 (Jorgensen et al. 2003). Low-resolution spectroscopy was also used to confirm that WT1190F, an object that may have orbited our planet from 1998 until it impacted Earth on November 13, 2015, was space debris (Micheli et al. 2018; Buzzoni et al. 2019), likely the translunar injection module of Lunar Prospector (Watson 2016). So far and out of three small bodies identified as temporarily captured, only one, 2020 CD₃, has been studied spectroscopically (Bolin et al. 2020).

The recently discovered object 2022 NX₁ (Bacci et al. 2022) follows an Earth-like orbit that turns it into a recurrent but

Send offprint requests to: R. de la Fuente Marcos, e-mail: rauldelafuentemarcos@ucm.es

[★] Based on observations made with the Gran Telescopio Canarias (GTC) telescope, in the Spanish Observatorio del Roque de los Muchachos of the Instituto de Astrofísica de Canarias (program ID GTC23-22A).

¹ <https://planet4589.org/space/gcat/>

² <https://conference.sdo.esoc.esa.int/proceedings/neosst1/paper/470>

ephemeral Earth companion (de la Fuente Marcos & de la Fuente Marcos 2022). It has been suggested that 2022 NX₁ could have an artificial origin or be lunar ejecta (Bacci et al. 2022). Here, we use reflectance spectroscopy and N -body simulations to determine the nature and actual origin of 2022 NX₁. This Letter is organized as follows. In Sect. 2, we introduce the context of our research, review our methodology, and present the data and tools used in our analyses. In Sect. 3, we apply our methodology to find out if 2022 NX₁ is natural or artificial and determine its probable origin. In Sect. 4, we discuss our results. Our conclusions are summarized in Sect. 5.

2. Context, methods, and data

In the following, we review some background material of theoretical nature needed to understand the results presented in the sections. Basic details of our approach and the data are also included here as well as a summary of the tools used to obtain the results.

2.1. Dynamics background

Earth-approaching objects may remain in its vicinity following geocentric orbits as captured satellites, when the value of the geocentric energy is negative (Carusi & Valsecchi 1979). In addition, they could be subjected to resonant behavior and become Earth co-orbitals trapped inside the 1:1 mean-motion resonance but following heliocentric paths, when the relative mean longitude of the object with respect to Earth (λ_r) oscillates about a fixed value (Morais & Morbidelli 2002). However, most visitors are just passing through and they are neither gravitationally captured by Earth nor engaged in the 1:1 orbital resonance with our planet.

Here and in order to classify capture events, we follow the terminology discussed by Fedorets et al. (2017): an object that does not complete at least one full revolution around Earth when bound is subjected to a temporarily captured flyby, but if it manages to complete at least one then we speak of a temporarily captured orbiter. On the other hand, if the value of λ_r oscillates about 180° , with an amplitude $>\pi$, the object follows a horseshoe trajectory with respect to Earth (Murray & Dermott 1999).

2.2. Methodology

Reflectance spectroscopy requires the observation of a target object (natural or artificial) and one or more well-studied solar analog stars at the same airmass as that of the object. The spectrum of the target is divided by the spectrum of the solar analog (by each one if two or more and the resulting spectra are averaged) to produce the final reflectance spectrum of the object under study. The entire data reduction process is described, for example, by Licandro et al. (2019) and it consists of bias and flat-field correction, background subtraction and extraction of the 1D spectrum from 2D images, and wavelength calibration.

The assessment of the past and future orbital evolution of an object and of its current dynamical state should be based on the analysis of results from a representative sample of N -body simulations that take the uncertainties in the orbit determination into account (see, for example, de la Fuente Marcos & de la Fuente Marcos 2018a, 2020). The near-Earth orbital domain is shaped by both mean-motion and secular resonances that may lead to a chaotic dynamical evolution (see, for example, Greenstreet et al. 2012) for both natural bodies and space debris even if the objects

Table 1. Values of the heliocentric Keplerian orbital elements and their respective 1σ uncertainties of 2022 NX₁.

Orbital parameter	value $\pm 1\sigma$ uncertainty
Semimajor axis, a (AU)	= 1.02192456 \pm 0.00000009
Eccentricity, e	= 0.02501797 \pm 0.00000006
Inclination, i ($^\circ$)	= 1.066697 \pm 0.000003
Longitude of the ascending node, Ω ($^\circ$)	= 274.76734 \pm 0.00011
Argument of perihelion, ω ($^\circ$)	= 169.58306 \pm 0.00011
Mean anomaly, M ($^\circ$)	= 65.0876 \pm 0.0002
Perihelion distance, q (AU)	= 0.99635808 \pm 0.00000007
Aphelion distance, Q (AU)	= 1.04749104 \pm 0.00000009
Absolute magnitude, H (mag)	= 28.1 \pm 0.8

Notes. The orbit determination of 2022 NX₁ is referred to epoch JD 2460000.5 (2023-Feb-25.0) TDB (Barycentric Dynamical Time, J2000.0 ecliptic and equinox), and it is based on 172 observations with a data-arc span of 142 days (solution date, November 21, 2022, 05:23:57 PST). Source: JPL’s SBDB.

involved do not experience deep close encounters with the Earth-Moon system and perhaps other planets. Statistical interpretation of the results is required if the evolution of the objects is unstable. If the quality of the orbit determination is not sufficiently robust and if the dynamical evolution is chaotic, predictions may only be reliable within a few decades (forward and backward in time) of the reference epoch.

2.3. Data, data sources, and tools

Object xkos033 was first observed by G. Duszanowicz and J. Camarasa using a 0.35-m, f/7.7 reflector telescope + CCD at Moonbase South Observatory in the Hakos mountains, Namibia on July 2, 2022; fifteen days later, it was announced with the provisional designation 2022 NX₁ (Bacci et al. 2022). The discovery Minor Planet Electronic Circular (MPEC) states that “The Earth-like orbit of the object and its orbital evolution suggest that it could be of an artificial origin, launched from the Earth decades ago or a lunar ejecta.”³

If 2022 NX₁ is a natural object, its orbit determination (see Table 1) makes it compatible with that of a near-Earth asteroid (NEA) of the Apollo dynamical class. Its most recent orbit determination is shown in Table 1; it is based on 172 observations with a data-arc span of 142 days and it has been retrieved from Jet Propulsion Laboratory’s (JPL) Small-Body Database (SBDB)⁴ provided by the Solar System Dynamics Group (SSDG, Giorgini 2011, 2015).⁵ The orbit determination is referred to standard epoch JD 2460000.5 TDB, which is also the origin of time in the calculations.

The N -body simulations carried out to study the orbital evolution of 2022 NX₁ have been performed using a direct N -body code developed by Aarseth (2003) that is publicly available from the website of the Institute of Astronomy of the University of Cambridge.⁶ This software applies the Hermite integration scheme formulated by Makino (1991). Results from this code were discussed in detail by de la Fuente Marcos & de la Fuente Marcos (2012). Calculations were carried out in an ecliptic coordinate system with the X axis pointing toward the first point of Aries or vernal equinox and in the ecliptic plane, the Z

³ <https://minorplanetcenter.net/mpec/K22/K22O04.html>

⁴ https://ssd.jpl.nasa.gov/tools/sbdb_lookup.html#/

⁵ <https://ssd.jpl.nasa.gov/>

⁶ <http://www.ast.cam.ac.uk/~sverre/web/pages/nbody.htm>

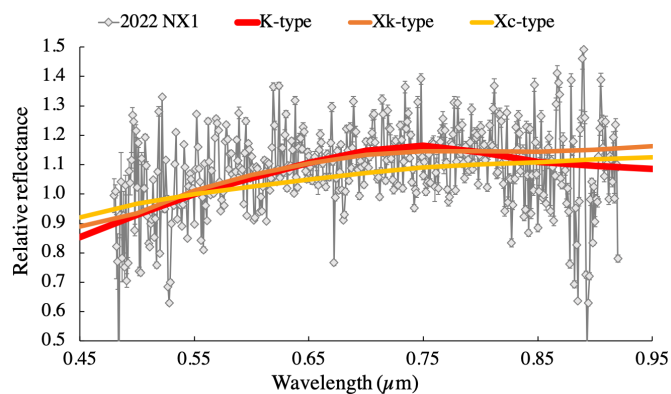


Fig. 1. Visible spectrum of 2022 NX₁ (gray) and its three best taxonomical classifications from the M4AST online tool, in decreasing order of goodness of fit: K type (in red), Xk type (in orange), and Xc type (in yellow).

axis perpendicular to the ecliptic plane and pointing northward, and the Y axis perpendicular to the previous two and defining a right-handed set. Our physical model included the perturbations by the eight major planets, the Moon, the barycenter of the Pluto-Charon system, and the three largest asteroids, (1) Ceres, (2) Pallas, and (4) Vesta. For accurate initial positions and velocities (see, for example, Sect. C), we used data from JPL’s SSDG Horizons online Solar System data and ephemeris computation service,⁷ which are based on the DE440/441 planetary ephemeris (Park et al. 2021). Most input data were retrieved from JPL’s SBDB and Horizons using tools provided by the Python package *Astroquery* (Ginsburg et al. 2019) and its *HorizonsClass* class.⁸

In order to interpret the reflectance spectrum of 2022 NX₁, we taxonomically classified it using the *Modeling for Asteroids (M4AST)*⁹ online tool (Popescu et al. 2012). Then, we compared it to other similar spectra of NEAs.

3. Results

In this section, we use reflectance spectroscopy and N -body simulations to determine the nature and actual origin of 2022 NX₁.

3.1. Spectroscopy

The visible spectrum of 2022 NX₁ was obtained on August 6, 2022, 23:40 UTC, using the Optical System for Imaging and Low Resolution Integrated Spectroscopy (OSIRIS) camera spectrograph (Cepa et al. 2000; Cepa 2010) at the 10.4 m Gran Telescopio Canarias (GTC), located at the El Roque de Los Muchachos Observatory (La Palma, Canary Islands). Observations were done under the program GTC23-22A (PI, J. de León). Details on the instrumental setup and the data reductions are provided in Appendix A.

The resulting spectrum is shown in Fig. 1 (gray line). The faintness of the target (apparent visual magnitude $m_V = 21.2$) and the fact that the observations were carried out under less than optimal observing conditions prevented us from using longer exposure times; therefore, extracted individual spectra had a low signal-to-noise ratio ($S/N \sim 30$). Nevertheless, it was good

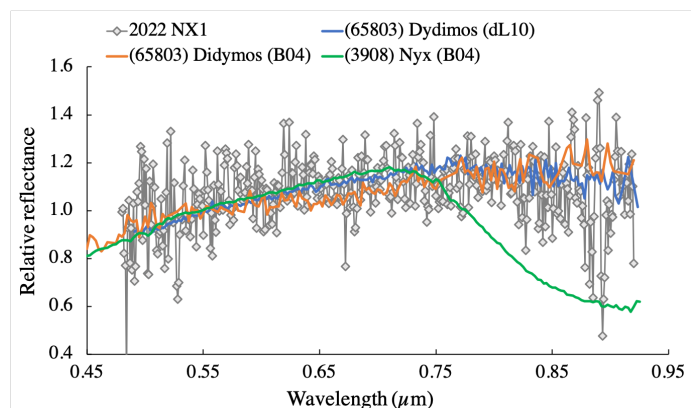


Fig. 2. Comparison between the visible spectrum of 2022 NX₁ (gray) and those of NEA (65803) Didymos from two different sources: B04, which classifies it as an X-type asteroid (orange, Binzel et al. 2004), and dL10, which classifies it as an S-type asteroid from its visible and NIR spectrum (blue, de León et al. 2010). We have also included the spectrum of one V-type asteroid (green, Binzel et al. 2004) as a comparison. The spectra have been normalized to unity at 0.55 μm .

enough to allow us to use the M4AST online tool to taxonomically classify it. The tool fits a curve to the data and compares it with the taxons defined by DeMeo et al. (2009) using a χ^2 fitting procedure. The three best results are provided, in order of decreasing goodness of fit. In this case, the best fit is with K-type asteroids, followed by Xk-type and Xc-type ones, as shown in Fig. 1. Considering the noise in the spectrum, the three classifications can be used to compositionally interpret the spectrum of 2022 NX₁, and so, the near-infrared (NIR, up to 2.5 μm) is needed to actually discern between them: K types have an almost neutral spectral slope in the NIR, with a wide and shallow absorption band at 1 μm (silicates), while Xk types have a red spectral slope in the NIR and a very slight absorption feature near 0.9 to 1 μm (intermediate between being carbonaceous like and silicate rich, with lower albedo values), and the Xc types show no feature around 1 μm and present a slightly curved and concave downward spectrum at NIR (carbonaceous like). It is important to remark here that having only the visible spectrum, we can only speculate on the subclasses of the X main taxon, and so, we can only conclude that the object’s visible spectrum fits both to a K-type and an X-type taxonomy.

An excellent example of the importance of having the NIR is the case of asteroid (65803) Didymos, which is a target of the Double Asteroid Redirection Test (DART) and Hera missions (see, for example, Cheng et al. 2016). Following the visible spectrum from Binzel et al. (2004), the object was classified as an Xk-type asteroid (orange line in Figure 2), but later observations that included the NIR (blue line in Figure 2) showed that the object is indeed an S-type asteroid (de León et al. 2010). We have also compared the spectrum of 2022 NX₁ with the spectra of several artificial objects, including space debris and satellites (see Fig. B.1 in Appendix B). Only one out of six spectra resembles that of 2022 NX₁, with the remaining five presenting a much redder spectral slope. Therefore, evidence points toward a natural origin for this object. Although we cannot determine the exact taxonomical class, it is evident that the object is not space debris but a NEA of the Apollo dynamical class. Considering its absolute magnitude in Table 1 and for typical values of the albedo of K types (range 0.08–0.29 according to Mainzer et al. 2011), 2022 NX₁ may have a size in the range 5 to 15 m. We note that Xk types, the second most likely taxonomy for 2022

⁷ <https://ssd.jpl.nasa.gov/horizons/>

⁸ <https://astroquery.readthedocs.io/en/latest/jplhorizons/jplhorizons.html>

⁹ <http://spectre.imcce.fr/m4ast/index.php/index/home>

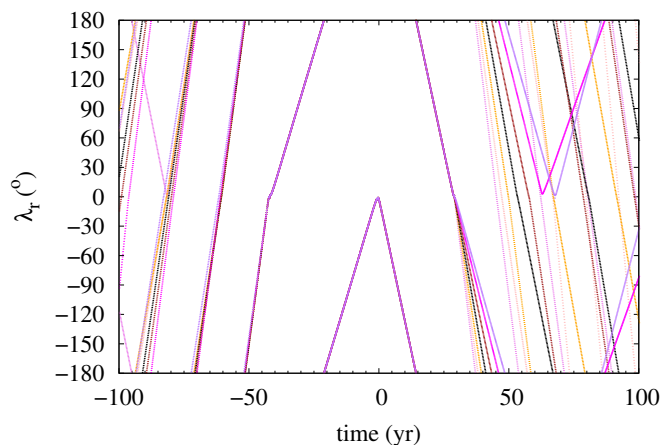


Fig. 3. Evolution of the relative mean longitude with respect to Earth, λ_r , of 2022 NX₁. The time interval (−100, 100) yr is shown. The figure shows results for the nominal solution (in black) as described by the orbit determination in Table 1 and those of control orbits or clones with Cartesian state vectors (see Appendix C) separated $+3\sigma$ (in brown), -3σ (in orange), $+6\sigma$ (in magenta), -6σ (in pink), $+9\sigma$ (in purple), and -9σ (in violet) from the nominal values in Table C.1. The output time-step size is 0.1 yr.

NX₁, have albedo values in the same range as those of K types, supporting our size estimation.

3.2. Orbital evolution

Apollo asteroid 2022 NX₁ experienced a close encounter with our planet at 0.00543 AU on June 26, 2022, well inside the Hill radius of Earth, 0.0098 AU, and at a relative velocity of just 0.96 km s^{−1}. Such a slow close encounter may lead to a temporary capture as in the case of 2020 CD₃ (de la Fuente Marcos & de la Fuente Marcos 2020). On the other hand, the orbit determination in Table 1 places this object close to the edge of Earth’s co-orbital zone that goes from ~ 0.994 AU to ~ 1.006 AU (see for example de la Fuente Marcos & de la Fuente Marcos 2018b). Therefore, and in addition to perhaps being temporarily bound to our planet, it may be moving co-orbital to it; in other words, the value of λ_r may be oscillating instead of circulating in the interval $(-\pi, \pi)$.

Figure 3 shows that 2022 NX₁ is currently co-orbital to Earth and follows a horseshoe path with λ_r librating about 180°. This is strictly true for any control orbit with Cartesian state vectors within $\pm 9\sigma$ from that of the nominal one. The data in the figure also show that the orbital evolution of this object is chaotic as its past becomes somewhat unpredictable for times earlier than 1981 (over 40 yr ago) and the same happens in the future, beyond 2051 (or nearly 30 yr from now). This asymmetry is the result of two close encounters with the Earth-Moon system on January 16, 1981, at 0.00417 AU and 1.15 km s^{−1} and on December 4, 2051, at 0.00303 AU and 1.39 km s^{−1}. Slow and deep encounters may result in temporary captures.

Figure 3 shows that, using the orbit determination in Table 1, 2022 NX₁ has a very short Lyapunov time, T_L (the inverse of the maximum Lyapunov exponent). The Lyapunov time is the characteristic timescale for the exponential divergence of initially close orbits. Figure 3 shows that T_L is about 40 yr for integrations into the past (30 yr for integrations into the future). However, for the Lyapunov time to reach an asymptotic value, a few thousand orbits are needed (see, for example, Lecer et al. 1992)

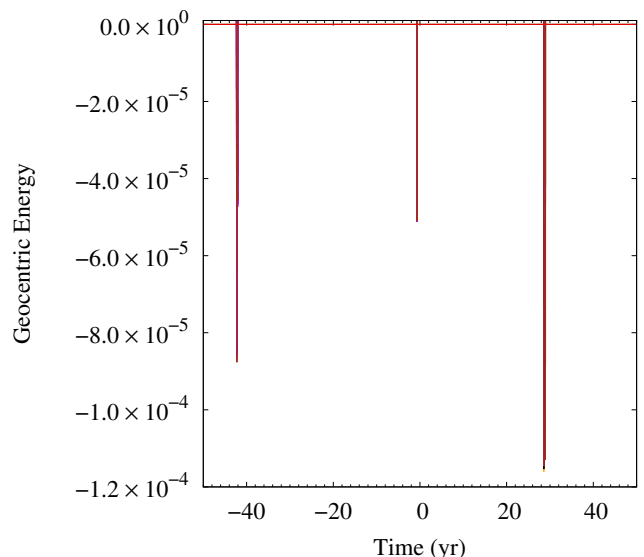


Fig. 4. Evolution of the value of the geocentric energy of 2022 NX₁. Captures happen when the value of the geocentric energy becomes negative. The unit of energy is such that the unit of mass is 1 M_\odot , the unit of distance is 1 AU, and the unit of time is one sidereal year divided by 2π . The evolution according to the nominal orbit in Table 1 is shown in black, and those of control or clone orbits with Cartesian vectors separated $\pm 3\sigma$ from the nominal values in Table C.1 are displayed in orange and brown, respectively.

and 2022 NX₁ experiences significant orbital changes on a much shorter timescale. The divergence of nearby post-encounter trajectories observed in Fig. 3 for the most recent close approach drives future resonant returns that may result in traversing a gravitational keyhole leading to a collision (see, for example, Valsecchi et al. 2003; Roa et al. 2021; Reddy et al. 2022). In fact and as of January 2023, 2022 NX₁ has a non-negligible Earth impact risk for approaches starting early in December of 2075.¹⁰

Figure 4 shows the evolution of the value of the geocentric energy of 2022 NX₁ in the interval of interest where all the control orbits produce consistent results. Capture events are not as deep and long as the ones experienced by 2020 CD₃ (de la Fuente Marcos & de la Fuente Marcos 2020). For this object, we do not observe events leading to moon-moon episodes in which the value of the selenocentric energy of 2022 NX₁ became negative as documented for 2020 CD₃ (de la Fuente Marcos & de la Fuente Marcos 2020). In this case, capture episodes are similar to those found for 1991 VG (see de la Fuente Marcos & de la Fuente Marcos 2018a).

Figure 5 shows the geocentric trajectories (in the XY plane, left panel, and the XZ plane, right panel) associated with the capture episodes identified in the time interval of ± 70 yr about the reference epoch, namely JD 2460000.5 TDB: January 1981, June 2022, and December 2051. These temporary capture episodes are robust and they appear during largely similar time windows for all the control orbits or clones studied here. The figure shows that all the episodes were of the temporarily captured flyby type; in other words, 2022 NX₁ did not complete even one revolution around our planet while its geocentric energy was negative. Although the most recent mini-moon episode, which lasted from June 11 until July 2 or 21 days, comprised a single temporary capture, the other two events included two captures each. The 1981 episode involved a 98 day-long event (from

¹⁰ [https://cneos.jpl.nasa.gov/sentry/details.html#?des=2022 NX1](https://cneos.jpl.nasa.gov/sentry/details.html#?des=2022%20NX1)

October 1, 1980, until January 7, 1981) and a subsequent, shorter one that lasted 29 days (from January 26, 1981, until February 24, 1981); the future 2051 episode will include 63 (from September 4, 2051, until November 6, 2051) and 52 day- (from January 2, 2052, until February 23, 2052) long captures. This is the first time a real object has been found to experience more than one capture event during the same close encounter with Earth. Asteroid 1991 VG may have experienced multiple temporarily captured flyby-type events though always simple (de la Fuente Marcos & de la Fuente Marcos 2018a), not double as in the case of 2022 NX₁.

Figure 3 shows that the current orbit determination of 2022 NX₁ does not allow for its orbital evolution to be predicted, beyond a few decades from the current epoch. It is therefore not possible to determine reliably how it may have reached NEA space. A hint of its possible source can be found in the results plotted in Fig. 6. Although the long-term evolution is chaotic and rather unstable, the value of the semimajor axis remains largely confined within 0.9478 AU (3:2 external resonance with Venus) and 1.3104 AU (3:2 external resonance with Earth). Therefore, and taking into account that 2022 NX₁ is probably a fragment of a larger NEA, we conjecture that it may have been formed in situ, within the NEA orbital realm during the last few hundred thousand years. On the other hand, we observe multiple (and sometimes lengthy) co-orbital episodes with Earth and relatively brief resonant engagements (when the value of a remains constant).

4. Discussion

The discovery MPEC of 2022 NX₁ (Bacci et al. 2022) suggested that it could have an artificial origin or be lunar ejecta. A number of captured objects —for example J002E3 and WT1190F— have been confirmed as space debris thanks to reflectance spectroscopy. However, the spectrum in Fig. 1 is inconsistent with those of spacecraft materials. On the other hand, Earth quasi-satellite (a co-orbital with λ_r librating about 0°, de la Fuente Marcos & de la Fuente Marcos 2016) 469219 Kamo‘oalewa (2016 HO₃) could be made of material consistent with what was found in lunar samples (Sharkey et al. 2021) and this provides support to the idea that some of the small bodies inhabiting the near-Earth orbital domain may have their origin on the Moon, likely as lunar ejecta. However, the reflectance spectrum discussed in Sect. 3 argues for a natural origin other than the Moon. It is also inconsistent with that of the only other mini-moon with available spectroscopy, 2020 CD₃, which is a V type (Bolin et al. 2020) such as asteroid (3908) Nyx (see green line in Fig. 2). In this context, the K-type spectrum of 2022 NX₁ argues for a diverse group of natural Earth co-orbitals with different origins and sources that probably reflects the spectral-type distribution of the NEA population (see, for example, Popescu et al. 2019). K-type asteroids, such as S types, contain rocky silicate minerals and are more common in the inner asteroid belt.

This is only the fourth time (after 1991 VG, 2006 RH₁₂₀, and 2020 CD₃) a minor body has been discovered during or right after experiencing an episode of temporary gravitational capture by Earth. As in previous cases, captures are linked to recurrent transient co-orbital motion, in particular of the horseshoe type (see for example de la Fuente Marcos & de la Fuente Marcos 2018a,b). While 2006 RH₁₂₀ and 2020 CD₃ were identified as temporary captures while still being bound to Earth (Kwiatkowski et al. 2009; de la Fuente Marcos & de la Fuente Marcos 2020), 1991 VG was not recognized as such until some time later (Tancredi 1997). The capture episodes experienced

by 1991 VG and 2022 NX₁ were rather similar (temporarily captured flybys); the same can be said about 2006 RH₁₂₀ and 2020 CD₃ (temporarily captured orbiters).

5. Summary and conclusions

In this Letter, we have presented spectroscopic observations of Earth’s horseshoe co-orbital and mini-moon 2022 NX₁ obtained on August 6, 2022, using the OSIRIS camera spectrograph at the 10.4 m GTC. We used the spectrum to characterize the object. We also carried out direct N -body simulations to investigate its orbital evolution. Our conclusions can be summarized as follows.

1. We confirm that 2022 NX₁ is a natural object but not lunar ejecta.
2. We find that 2022 NX₁ has a visible spectrum consistent with that of a K-type asteroid, although it could also be classified as an Xk type.
3. We identify two robust, short episodes of the temporarily captured flyby type for 2022 NX₁ in 1981 and 2022, and predict a third one that will take place in 2051. The temporary capture episodes in 1981 and 2051 include two separate events each.
4. Considering its absolute magnitude and for typical values of the albedo of K-type asteroids, 2022 NX₁ may have a size in the range 5 to 15 m that makes it the largest known mini-moon. This result remains valid if it is an Xk-type asteroid.
5. We confirm that 2022 NX₁ inhabits the rim of Earth’s co-orbital space, the 1:1 mean-motion resonance, and experiences recurrent co-orbital episodes of the horseshoe type as previous mini-moons did. It is currently following a horseshoe path with respect to Earth.
6. The current orbit determination of 2022 NX₁ is not robust enough to reconstruct its past and future orbital evolution beyond ± 50 yr from the current epoch.

Considering its relatively small size and its probable long-term dynamical evolution into the past, we conjecture that 2022 NX₁ may have formed via fragmentation within NEA orbital parameter space during the last few hundred thousand years. This preliminary interpretation is based on the currently available data and may change as the orbit determination accuracy improves.

Acknowledgements. We thank an anonymous reviewer for a quick and particularly constructive report. RdIFM and CdIFM thank S. J. Aarseth for providing one of the codes used in this research and A. I. Gómez de Castro for providing access to computing facilities. JdL acknowledges support from the ACISI, Consejería de Economía, Conocimiento y Empleo del Gobierno de Canarias and the European Regional Development Fund (ERDF) under grant with reference ProID2021010134. JdL also acknowledges financial support from the Spanish Ministry of Science and Innovation (MICINN) through the Spanish State Research Agency, under Severo Ochoa Programme 2020-2023 (CEX2019-000920-S). This work was partially supported by the Spanish ‘Agencia Estatal de Investigación (Ministerio de Ciencia e Innovación)’ under grant PID2020-116726RB-I00 /AEI/10.13039/501100011033. Based on observations made with the Gran Telescopio Canarias (GTC), installed at the Spanish Observatorio del Roque de los Muchachos of the Instituto de Astrofísica de Canarias, on the island of La Palma. This work is partly based on data obtained with the instrument OSIRIS, built by a Consortium led by the Instituto de Astrofísica de Canarias in collaboration with the Instituto de Astronomía de la Universidad Nacional Autónoma de México. OSIRIS was funded by GRANTECAN and the National Plan of Astronomy and Astrophysics of the Spanish Government. In preparation of this Letter, we made use of the NASA Astrophysics Data System, the ASTRO-PH e-print server, and the MPC data server.

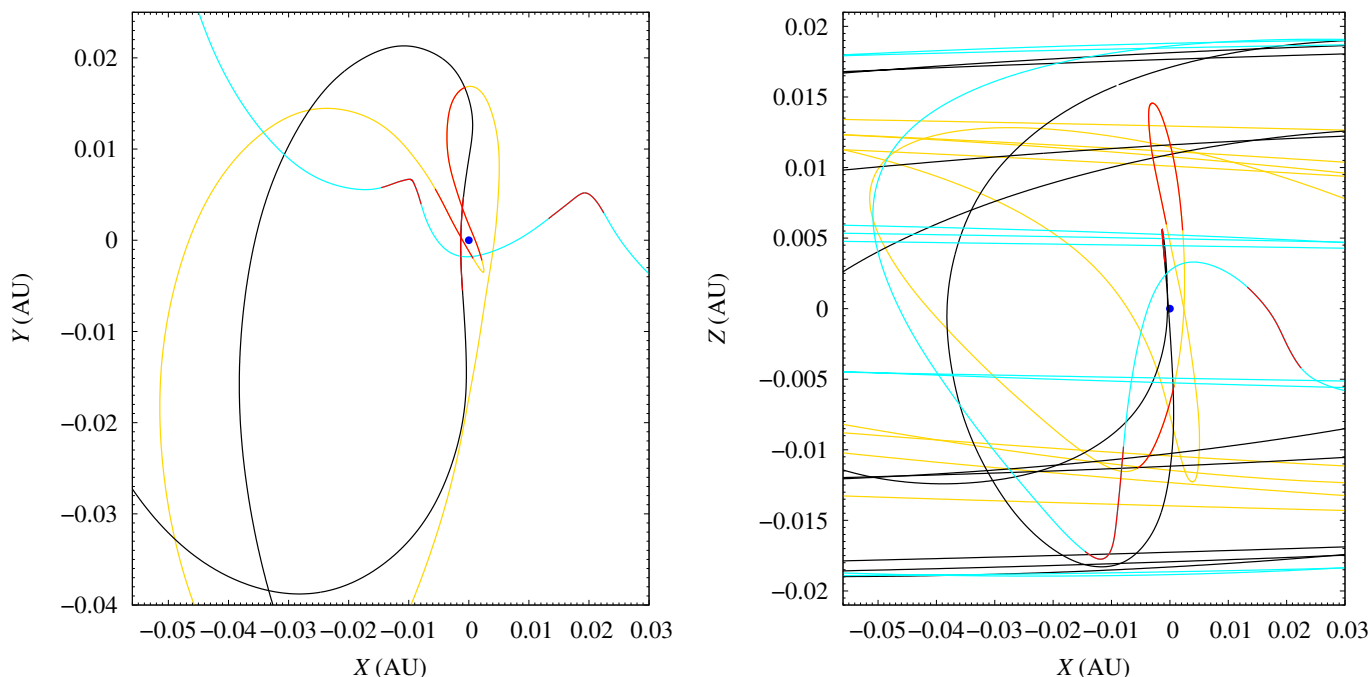


Fig. 5. Geocentric trajectories of 2022 NX₁ during the mini-moon episodes. The flyby in 1981 appears in gold, the one that occurred in 2022 is in black, and the future flyby in 2051 is in cyan. The part of the trajectory for which the geocentric energy becomes negative is always displayed in red. Earth is represented by a blue dot.

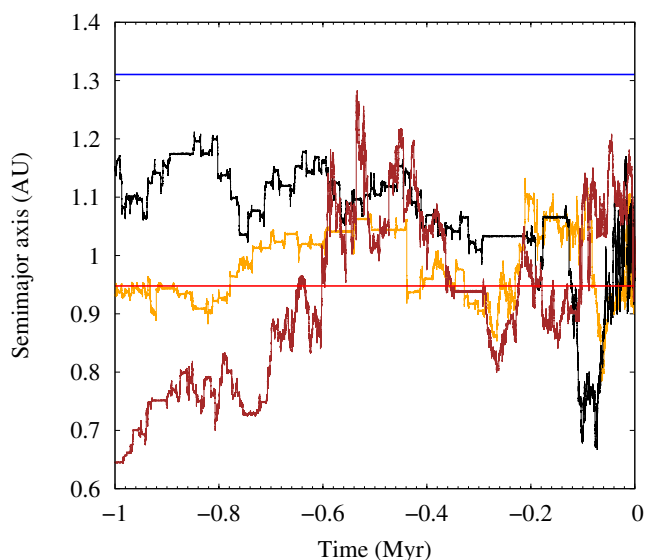


Fig. 6. Evolution of the value of the semimajor axis of 2022 NX₁. The evolution according to the nominal orbit in Table 1 is shown in black and those of control or clone orbits with Cartesian vectors separated $\pm 3\sigma$ from the nominal values in Table C.1 are displayed in orange and brown, respectively. In red, we signal the location of the 3:2 external resonance with Venus at 0.9478 AU, and in blue we show the location of the 3:2 external resonance with Earth at 1.3104 AU.

References

Aarseth, S. J. 2003, *Gravitational N-Body Simulations* (Cambridge: Cambridge University Press), 27

Astropy Collaboration, Robitaille, T. P., Tollerud, E. J., et al. 2013, *A&A*, 558, A33

Astropy Collaboration, Price-Whelan, A. M., Sipőcz, B. M., et al. 2018, *AJ*, 156, 123

Bacci, P., Maestriperri, M., Grazia, M. D. 2022, *Minor Planet Electronic Circulars*, 2022-O04

Binzel, R. P., Perozzi, E., Rivkin, A. S., et al. 2004, *Meteorit. Planet. Sci.*, 39, 351

Bolin, B., Jedicke, R., Granvik, M., et al. 2014, *Icarus*, 241, 280

Bolin, B. T., Fremling, C., Holt, T. R., et al. 2020, *ApJ*, 900, L45

Buzzoni, A., Altavilla, G., Fan, S., et al. 2019, *Advances in Space Research*, 63, 371

Cano, J. L., Ceccaroni, M., Faggioli, L., et al. 2019, *ESA's Activities on the Boundaries between NEO and Debris Detection*, in *1st NEO and Debris Detection Conference*, ed. T. Flohrer, R. Jehn, & F. Schmitz (ESA Space Safety Programme Office Publishing), 470

Carusi, A. & Valsecchi, G. B. 1979, *Riunione della Societa Astronomica Italiana*, 22, 181

Cepa, J., Aguiar, M., Escalera, V. G., et al. 2000, *Proc. SPIE*, 4008, 623

Cepa, J. 2010, *Astrophysics and Space Science Proceedings*, 14, 15

Cheng, A. F., Michel, P., Jutzi, M., et al. 2016, *Planet. Space Sci.*, 121, 27

Cowardin, H. M., Hostetler, J. M., Murray, J. I., et al. 2021, *Journal of the Astronomical Sciences*, 68, 1186

de la Fuente Marcos, C. & de la Fuente Marcos, R. 2012, *MNRAS*, 427, 728

de la Fuente Marcos, C. & de la Fuente Marcos, R. 2016, *MNRAS*, 462, 3441

de la Fuente Marcos, C. & de la Fuente Marcos, R. 2018a, *MNRAS*, 473, 2939

de la Fuente Marcos, C. & de la Fuente Marcos, R. 2018b, *MNRAS*, 473, 3434

de la Fuente Marcos, C. & de la Fuente Marcos, R. 2020, *MNRAS*, 494, 1089

de la Fuente Marcos, C. & de la Fuente Marcos, R. 2022, *Research Notes of the American Astronomical Society*, 6, 160

de León, J., Licandro, J., Serra-Ricart, M., et al. 2010, *A&A*, 517, A23

DeMeo, F., Binzel, R. P., Slivan, S. M., et al. 2009, *Icarus*, 202, 160

Fedorets, G., Granvik, M., & Jedicke, R. 2017, *Icarus*, 285, 83

Fedorets, G., Micheli, M., Jedicke, R., et al. 2020, *AJ*, 160, 277

Ginsburg, A., Sipőcz, B. M., Brasseur, C. E., et al. 2019, *AJ*, 157, 98

Giorgini, J. 2011, in *Journées Systèmes de Référence Spatio-temporels 2010*, ed. N. Capitaine, 87–87

Giorgini, J. D. 2015, *IAUGA*, 22, 2256293

Granvik, M., Vaubaillon, J., & Jedicke, R. 2012, *Icarus*, 218, 262

Greenstreet, S., Ngo, H., & Gladman, B., 2012, *Icarus*, 217, 355

Jorgensen, K. M. 2000, Ph.D. Thesis, University of Colorado, Boulder

Jorgensen, K., Rivkin, A., Binzel, R., et al. 2003, *American Astronomical Society, DPS meeting #35*, id.36.02

Jorgensen, K., Africano, J., Hamada, K., et al. 2004, *Advances in Space Research*, 34, 1021

Kwiatkowski, T., Kryszczyńska, A., Polińska, M., et al. 2009, *A&A*, 495, 967

Lecar, M., Franklin, F., & Murison, M. 1992, *AJ*, 104, 1230

- Licandro, J., de la Fuente Marcos, C., de la Fuente Marcos, R., et al. 2019, *A&A*, 625, A133
- Mainzer, A., Grav, T., Masiero, J., et al. 2011, *ApJ*, 741, 90
- Makino, J. 1991, *ApJ*, 369, 200
- McDowell, J. C., 2020, General Catalog of Artificial Space Objects, Release 1.2.12, <https://planet4589.org/space/gcat>
- Micheli, M., Buzzoni, A., Koschny, D., et al. 2018, *Icarus*, 304, 4
- Morais, M. H. M. & Morbidelli, A. 2002, *Icarus*, 160, 1
- Murray, C. D., & Dermott, S. F. 1999, *Solar System Dynamics* (Cambridge: Cambridge University Press)
- Park, R. S., Folkner, W. M., Williams, J. G., et al. 2021, *AJ*, 161, 105
- Popescu, M., Birlan, M., & Nedelcu, D. A. 2012, *A&A*, 544, A130
- Popescu, M., Vaduvescu, O., de León, J., et al. 2019, *A&A*, 627, A124
- Reddy, V., Kelley, M. S., Dotson, J., et al. 2022, *PSJ*, 3, 123
- Roa, J., Farnocchia, D., & Chesley, S. R. 2021, *AJ*, 162, 277
- Schildknecht, T. 2007, *A&A Rev.*, 14, 41
- Sharkey, B. N. L., Reddy, V., Malhotra, R., et al. 2021, *Communications Earth and Environment*, 2, 231
- Tancredi, G. 1997, *Celestial Mechanics and Dynamical Astronomy*, 69, 119
- Valsecchi, G. B., Milani, A., Gronchi, G. F., et al. 2003, *A&A*, 408, 1179
- Vananti, A., Schildknecht, T., & Krag, H. 2017, *Advances in Space Research*, 59, 2488
- Watson, T. 2016, *Nature*, 19162

Appendix A: Spectroscopic observations and data reduction

We used the OSIRIS camera spectrograph at the 10.4 m GTC. The OSIRIS detector is a mosaic of two Marconi 2048×4096 pixel CCDs, with a plate scale of 0.127"/pixel that provides a field of view of 7.8'×7.8'. The standard operation mode of the instrument uses a 2×2 binning. We used the R300R grism that covers a wavelength range from 0.48 to 0.92 μm , with a dispersion of 7.74 $\text{\AA}/\text{pixel}$ for a 0.6" slit. Weather conditions during the observations were less than optimal. Although there were no clouds, the seeing was variable, ranging from 1.0" to 1.5". We therefore used the 1.2" slit, oriented to the parallactic angle, and with the tracking of the telescope at a set rate matching the proper motion of the asteroid. We obtained two consecutive spectra of 300 s of exposure time each, at an airmass of 1.15, offsetting the telescope 10" in the slit direction between the spectra. To obtain the reflectance spectra of the asteroid, we also observed two solar analog stars (Landolt SA 110-361 and SA 102-1081), using the same instrumental configuration as for the asteroid, and at a similar airmass. In the case of the stars, we obtained three individual spectra, also offsetting the telescope in the slit direction by 10" between individual spectra. Spectral images of the asteroid and the solar analog stars were bias and flat-field corrected. The 2D spectra were background subtracted and collapsed to 1D by adding all the flux within an aperture (typically defined as the distance from the center of the spatial profile where the intensity is 10% of the peak intensity). One-dimensional spectra were then wavelength calibrated using Xe+Ne+HgAr arc lamps. We added the two asteroid spectra and averaged, for each solar analog, their corresponding individual spectra. Then, as a final step, we divided the spectrum of the asteroid by the spectrum of each solar analog star, and averaged the two resulting ratios to compute values and error bars. That is the final spectrum shown in Fig. 1.

Appendix B: Reflectance spectra of artificial objects

We have collected published spectra of several artificial objects and put them together with our visible spectrum of 2022 NX₁ in Fig. B.1. We included several rocket bodies that launched in different years (Rocket 1965, 1981, and 1996), and a satellite, from Jorgensen et al. (2004); the Meteosat satellite and the debris object E08152A in an elliptical geosynchronous equatorial orbit, from Vananti et al. (2017); and the artificial object WT1190F, from Micheli et al. (2018). As it can be seen, the majority of artificial objects present visible spectra with a much redder spectral slope compared to that of 2022 NX₁. We have found only one rocket body (Rocket 1981) with a similar spectrum to that of 2022 NX₁.

NEA 2022 NX₁ experienced a close approach to Earth at 0.004 AU on January 16, 1981. The artificial satellites Kosmos 1238¹¹ and Kosmos 1239¹² were launched from Plesetsk on that day. Kosmos 1238 was placed in a low-Earth orbit by a two-stage Kosmos-3M rocket and Kosmos 1239 by a three-stage Soyuz-U rocket. Both satellites were successfully placed in nearly polar orbits. The timings of the close approach of 2022 NX₁ and the launch of Kosmos 1239 are somewhat con-

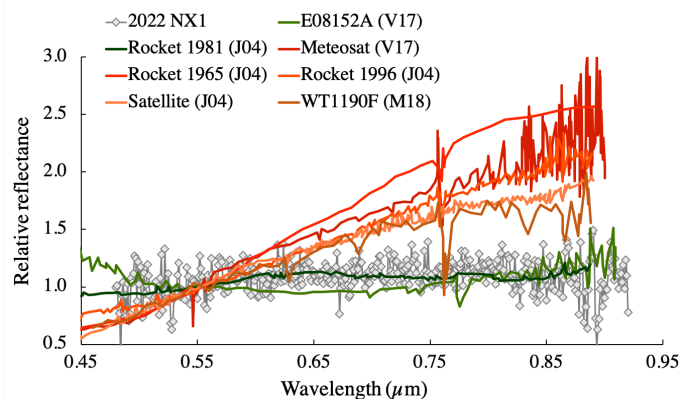


Fig. B.1. Visible spectrum of 2022 NX₁ compared with visible spectra of different artificial objects, including rocket bodies, satellites, and space debris, from several sources: J04 (Jorgensen et al. 2004); V17 (Vananti et al. 2017); and M18 (Micheli et al. 2018). The spectra have been normalized to unity at 0.55 μm .

Table C.1. Barycentric Cartesian state vector of 2022 NX₁: components and associated 1σ uncertainties.

Component	value $\pm 1\sigma$ uncertainty
X (AU)	$= -9.027005168802194 \times 10^{-1} \pm 1.15841197 \times 10^{-7}$
Y (AU)	$= 4.734562771552952 \times 10^{-1} \pm 2.20475306 \times 10^{-7}$
Z (AU)	$= -1.563722540015655 \times 10^{-2} \pm 2.51735401 \times 10^{-8}$
V_X (AU/d)	$= -8.392947703131247 \times 10^{-3} \pm 2.25199602 \times 10^{-9}$
V_Y (AU/d)	$= -1.500620447456039 \times 10^{-2} \pm 3.23298503 \times 10^{-9}$
V_Z (AU/d)	$= -1.789369608185863 \times 10^{-4} \pm 9.62976703 \times 10^{-10}$

Notes. Data are referred to epoch JD 2460000.5, which corresponds to 0:00 on February 25, 2023, TDB (J2000.0 ecliptic and equinox). Source: JPL's Horizons.

sistent. Rocket 1981 from Jorgensen et al. (2004) seems to be made of aluminum in white paint; the Soyuz-U rocket that launched Kosmos 1239 was painted mostly whitish in color. Although there is a series of curious coincidences, we consider it highly unlikely that one of the stages of the Soyuz-U rocket that launched Kosmos 1239 may have been able to escape Earth's gravity to reach a heliocentric (but co-orbital to Earth) and low-inclination orbit, and eventually return for another close approach on June 26, 2022.

Appendix C: Input data

Here, we include the barycentric Cartesian state vector of NEA 2022 NX₁. This vector and its uncertainties have been used to perform the calculations discussed above and to generate the figure that displays the time evolution of the critical angle, λ_r . For example, a new value of the X component of the state vector is computed as $X_c = X + \sigma_X r$, where r is an univariate Gaussian random number, and X and σ_X are the mean value and its 1σ uncertainty in Table C.1.

¹¹ <https://nssdc.gsfc.nasa.gov/nmc/spacecraft/display.action?id=1981-003A>

¹² <https://nssdc.gsfc.nasa.gov/nmc/spacecraft/display.action?id=1981-004A>